

# Electron-Hadron shower discrimination in a liquid argon time projection chamber

J.J. Back, G.J. Barker, A.J. Bennieston, S.B. Boyd, B. Morgan, and Y.A. Ramachers\*  
*Dept. of Physics, University of Warwick, Coventry CV4 7AL, UK*

By exploiting structural differences between electromagnetic and hadronic showers in a multivariate analysis we present an efficient Electron-Hadron discrimination algorithm for liquid argon time projection chambers.

PACS numbers: 95.55.Vj, 13.15.+g, 29.85.Fj

## I. INTRODUCTION

Liquid Argon Time Projection Chambers (LAr-TPCs) are recognised as being a potential detector technology for a next-generation Neutrino oscillation experiment and their development is the subject of vibrant R&D programmes in Europe, Japan and the USA (see Ref. [1] and references therein). The simultaneous tracking and calorimetry capability, with millimetric granularity, makes LAr-TPCs ideal to image Neutrino interactions over a wide range of energies as demonstrated recently by ICARUS [2].

Despite the physics promise of LAr-TPCs, a fully automated (that is, with zero human interaction) software system for reconstructing events has proven difficult to achieve. With the availability of more and more event data, recent years have seen progress in limited clustering of structures and tracking. However, a general event is likely to contain a mixture of showers and tracks originating from an unknown vertex anywhere in the sensitive volume. One major challenge for automated reconstruction is to disentangle the fundamentally different shower and track structures and hence segment the event into its constituent final states. Accurate segmentation is critical for subsequent particle identification on the substructures and final classification of the interaction. Neutrino oscillation analyses proposed for next-generation facilities rely heavily on accurate interaction classification, motivating studies of this task.

In this article, we concentrate on the particle identification step assuming exact segmentation, deferring discussion of techniques for this more challenging task to later publications. We present a study using a set of effective and computationally simple variables which allow the discrimination of Electron shower structures from all relevant hadronic shower structures in a fine-grained tracking detector such as a LAr-TPC. For the intended physics application, the dominant Hadron shower structures result from Pions, Protons or Kaons in the final state. In this context, Electron-Hadron shower discrimination is important for Neutrino oscillation studies in order to measure Electron-neutrino events in a Muon-neutrino beam, resulting in an energetic Electron in the

LAr medium after a charged-current interaction with a nucleus. Therefore, the Electron is considered to be the “signal” and anything non-electron, i.e. Hadron showers, is labelled as “background”, unless stated otherwise.

Additionally, the energy resolution of any LAr-TPC will depend on the nature of the particle depositing energy due to quenching factors. Electromagnetic and hadronic particle energy depositions will each require separate energy calibrations. Stronger ionising particles such as Hadrons would show particle specific relative quenching factors (relative to Electrons), hence for their energy measurement particle identification would be beneficial.

The set of variables also prove to be useful for other particle identification tasks. Track structures associated with Protons or Muons can be identified by these variables as well as, to a lesser extent, hadronic final states such as neutral and charged Pions and Kaons.

In the following, we describe the analysis algorithm by first introducing the discrimination variables and then presenting their applicability to identifying particles in various Neutrino interaction event topologies.

## II. ELECTRON-SHOWER DISCRIMINATION ALGORITHM

Below, we detail the calculation and physics motivation of six discriminating variables. The main assumption underpinning all of the following is that clustered energy deposits, hits, in the detector from a particular particle have been collected as a single object by the reconstruction, i.e. a cluster.

This crucial first step of any LAr detector analysis is assumed to have taken place already. It should be stressed that a reliable, complete and automatic initial clustering step is, in fact, among the unsolved challenges of LAr data analysis, owing to the richness of topological event structures in such a detector, and will not be addressed here.

The first step of the discrimination algorithm consists of transforming the isolated cluster using a principal component analysis (PCA) [3]. The data at this stage consists purely of detector hits forming a point-cloud of unknown shape. Dealing with LAr detectors translates into the capability of assigning three spatial coordinates and a charge value to each individual hit (with corresponding

---

\*Corresponding author: y.a.ramachers@warwick.ac.uk

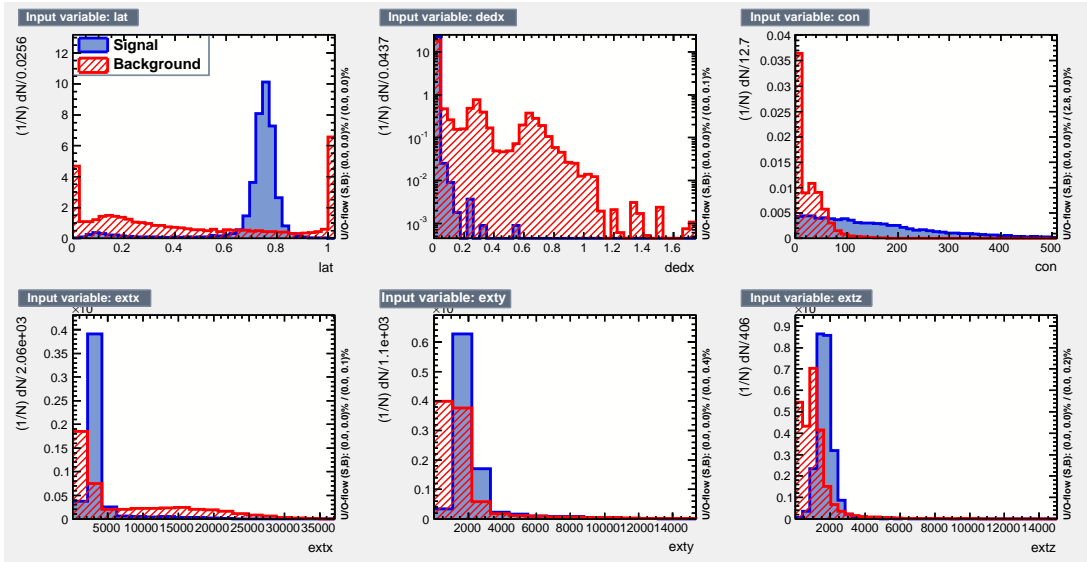


FIG. 1: The set of six discrimination variables applied to the CN2PY beam (see text) Neutrino events. Signal events are defined as electromagnetic shower events from Electrons, compared to the complete shower background, which includes all simulated structures from Protons, charged Pions, neutral Pions, charged and neutral Kaons and Muons, all with appropriate weighting factors. The vertical text on the right-hand side indicates the under- and overflows [4].

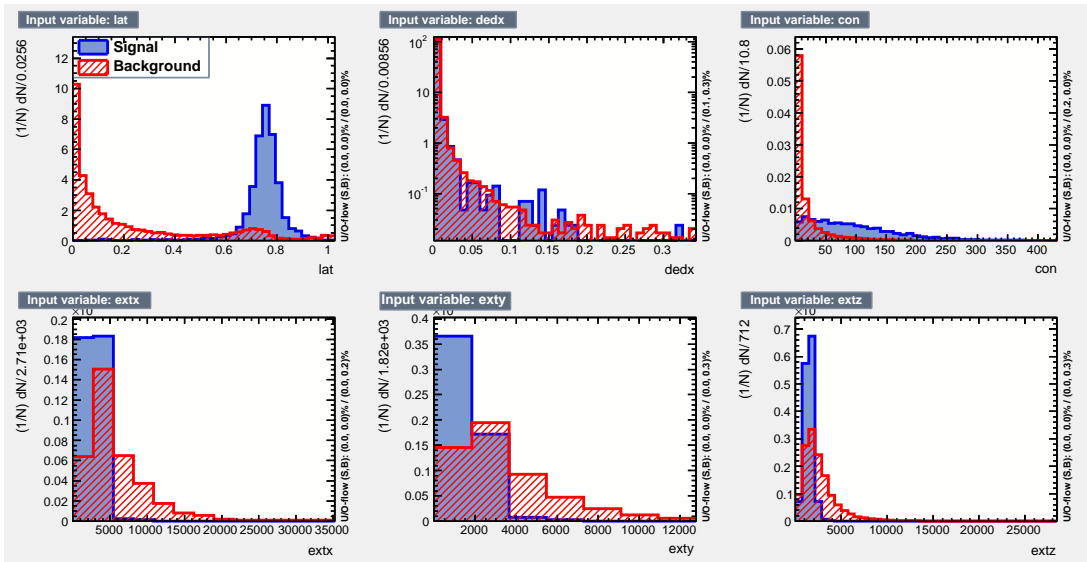


FIG. 2: Similar to Fig. 1; the set of six discrimination variables here applied to uniform energy final state particles, sampled from 10 MeV to 4.5 GeV.

uncertainties).

The reason for the initial PCA step is that it allows us to consider the unknown point-cloud to be aligned and ordered in a consistent way. The PCA is set up such that it calculates the three principal spatial components (ignoring the charge of the hit) as eigenvalues of the transformation matrix, which itself consists of the corresponding eigenvectors. Applying the transformation aligns the coordinate axes to the principal axes. This allows to utilise

transverse and longitudinal geometric information due to the presence of a well defined axis for the structure.

#### A. The lateral projection variable “lat”

This discrimination variable is motivated by previous and ongoing accelerator experiments and their analysis of electromagnetic (EM) and Pion showers (see for example

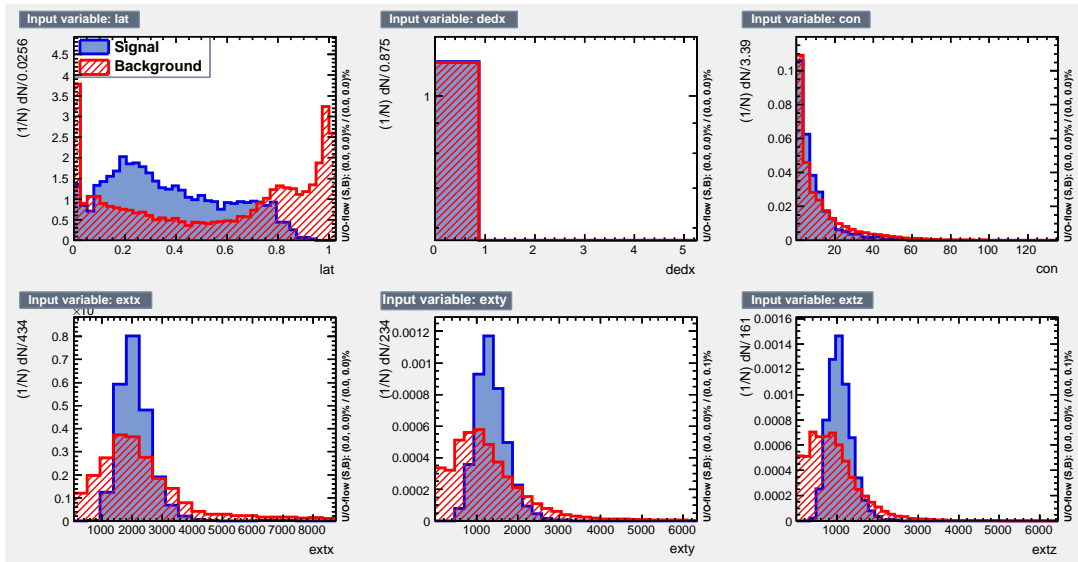


FIG. 3: Similar to Fig. 1; the set of six discrimination variables here applied to uniform energy final state particles, sampled from 10 MeV to 770 MeV.

Ref. [5]). The entire point-cloud is projected onto the plane of minor principal components (the lateral plane to the major principal axis). A core region is defined around the projected mean value and the ratio of energy (charge) deposited in the core to the total energy (charge) yields the “lat” variable.

Charged Hadron showers tend to have a denser core region compared to EM showers, or often resemble a track-like structure with only a thin “halo” around it, or dissolve into a wide-spread cloud of hits. Proton tracks might or might not shower at all. EM showers, by contrast, tend to produce more constant halo-to-core ratios, as shown in Fig. 1.

The precise definition of the core region turns out to be non-critical. For simplicity, a circular shape is chosen, which is centred on the mean value of the projected point-cloud and is defined with the Molière radius in liquid argon, which is equal to 9.61 cm [6]. Each hit inside the core contributes to the sum of energy in the core, which is then divided by the total energy of the shower (the sum of the energies of all hits).

### B. The hit concentration variable “con”

While the previous variable emphasises a subdivision of the shower structure into two main components (core and halo), the hit concentration variable “con” attempts to use the same lateral information globally. This is independent of any material constant, such as the Molière radius.

The variable first calculates the radial distance of each hit from the main principal axis, i.e. the radial distance from the origin in the lateral projection plane. A

minimum threshold radius is set in order to avoid the Coulomb singularity (for practical purposes chosen as 1 mm in this analysis), and finally the hit concentration is calculated as the sum of charge (energy) of the hits divided by their radial distance.

The idea is to calculate the Coulomb potential energy of the point-cloud around the main principal axis. This approach delivers complementary information to the previous rigid division into two parts, since it emphasises the extremes such as track-like structures as being particularly highly concentrated, and very loose structures as being particularly low in concentration. Figures 1, 2 and 3 show the main benefit of this variable. The Hadron showers are dominated by less densely concentrated structures (they peak at low Coulomb energies around the main principal axis). A second population of Hadron events contain Proton tracks as well as sufficiently dense Pion tracks, contributing a large value to this concentration variable. EM showers are rather non-specific but are significantly more concentrated than Hadron showers.

### C. Initial ionisation loss variable “dedx”

The above two variables already provide excellent EM/Hadron shower discrimination potential. This third variable is mainly introduced to improve the low energy discrimination of the analysis, enabling additional applications of the procedure.

This variable attempts to use the information about the longitudinal shower characteristics. At Hadron colliders the entire longitudinal shower profile is used [5], but it was found that only the first part of any shower is necessary for providing discrimination at low energies.

This variable is ineffective at high primary particle energies and could be dropped since the ionisation loss curves of final state particles become indistinguishable.

The calculation proceeds as follows: partition the entire set of hits into roughly equal parts in hit numbers and consider only the first slice. This slicing is particularly simple after the PCA and hit ordering. The first slice then contains hits from the start of the shower. Then, calculate the sum of charges (energies) contained in the slice, its physical length along the major principal axis and build the specific energy loss variable  $dE/dx$ , normalised to the number of hits in the slice. For quantitative comparisons, energies were normalised to the liquid argon critical energy of 30.6 MeV and lengths to the specific radiation length of 14 cm [6].

The number of slices is fixed to 50, since fewer slices provide less discriminating power, while too many slices diminish the number of available hits in each slice, enhancing statistical fluctuations. Typically, each slice would contain more than 40 hits, sometimes increasing to several hundred hits for large showers, depending on the particle energy.

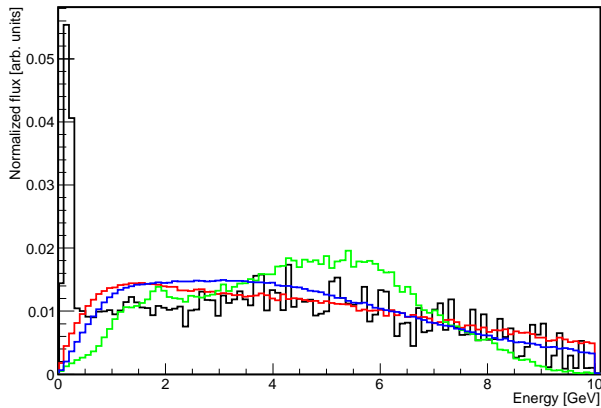


FIG. 4: The normalised CN2PY Neutrino beam fluxes [10] from negative Pion decays. The black line shows the Muon-neutrino flux; red - the Electron-neutrino flux; green - anti-Muon-neutrino flux and blue - anti-Electron-neutrino flux.

As expected, this variable delivers additional discrimination power against low energy Protons with relatively large specific ionisation energy loss compared to Pions, Electrons and Muons. It might also support distinguishing low energy heavy charged fragments and their corresponding showers. At high primary Neutrino energies, this variable becomes ineffective, since the resulting Proton energies are generally high enough not to be easily distinguishable according to their ionisation energy loss (and Pions even less so). Note that the discrimination power of this variable is not clearly visible in Fig. 3. Due to the low energies of final state particles in this case, the calculation would fail (too few hits in a slice) and the variable does not contribute to the analysis in these

cases. The rigid definition from above would have to be optimised further for such a low energy study.

#### D. Spatial extent variables “ext<sub>x,y,z</sub>”

The final three proposed discrimination variables are obtained by quantifying the spatial extent of the hit cloud in the three available principal component axes. A definition of the extent in purely geometrical terms turns out to be very useful.

The spatial extent is calculated by obtaining the convex hull in 3D around the hit cloud and finding the maximum distance (extent) of the hull on all three axes. Building the convex hull around an object is a standard algorithm in image analysis [7]. Even though its application in 3D is rather exotic, ready-made implementations of the code exist, for instance in the scientific python library, SciPy [8]. The meaning of the term convex hull can be visualised by considering stiff packaging paper, wrapped around an irregularly shaped object, i.e. the hit cloud, in order to enclose it completely. The paper would represent the convex hull, without the folds and overlaps real paper would produce.

The convex hull is obtained by calculating the Delaunay tessellation [7] of the hit cloud and finding the outermost Delaunay triangles, made of data members, enveloping the entire cloud. The difference between the maximum and minimum distance on each (principal component) coordinate axes is calculated, giving the extent of the hull in all three dimensions.

### III. RESULTS

Several simulated single particle event classes were prepared as input to the analysis. We have tested the algorithm with a Muon-neutrino flux generated as part of the LAGUNA-LBNO FP7 programme [9] to evaluate the physics potential of a long baseline experiment between CERN and an underground far detector location in Pyhasalmi Finland (CN2PY). The CN2PY Neutrino flux [10] (un-oscillated) from decaying negatively charged Pions (for a distance of 2300 km) provided the input for the first case study. Neutrino reaction final states were produced using the GENIE event generator [11]. The normalised Neutrino energy distributions are shown in Fig. 4 with relative weighting factors given in Table I.

TABLE I: The relative weighting factors for the CN2PY Neutrino beam (un-oscillated) from negatively charged Pions taken as input for this study.

$\bar{\nu}_\mu$ flux	$\nu_\mu$ flux	$\bar{\nu}_e$ flux	$\nu_e$ flux
1.0	$3.471 \times 10^{-2}$	$4.455 \times 10^{-3}$	$1.0772 \times 10^{-3}$

The GENIE simulated events were un-filtered, with all possible final state particles allowed. The total number of each individual particle final state from GENIE in each of the four Neutrino fluxes then results in individual weighting factors for that particle species during the subsequent analysis. The complete set of weighting factors is listed in Table II. Final state Hadrons which do not decay by default in Geant4 have been ignored in the subsequent analysis.

These single particle energy distributions from the GENIE simulations then serve as the particle source in the Geant4 Monte-Carlo transport simulation toolkit [12]. The simulation models an homogeneous liquid argon detector as a cylinder with a radius and height of 100 m, in order to fully contain the showers. Particles start at the centre of the cylindrical volume and are tracked through the volume with interactions modelled by the QGSP\_BIC\_HP physics list, with all electromagnetic and hadronic processes enabled. The LAr volume is divided into  $(1 \times 1 \times 1)$  mm<sup>3</sup> cubic voxels, and all primary and secondary particles are tracked through voxels down to zero energy, or until they leave the volume. Energy deposits by charged particles passing through voxels are tallied into a map between voxel coordinates and the total energy deposited. No attempt was made to model the readout system, but quenching of ionisation events specific to LAr detectors was taken into account following [13].

Results are collected and processed in a final step by four selected multivariate analysis algorithms (MVA) taken from the TMVA toolkit [4]. Each MVA is based on supervised learning, requiring separate training and test data samples. Each sample is chosen from a random split in half of the available data. The final evaluation delivers optimal cuts for each selected MVA method, producing efficiencies for signal selection, background selection and corresponding purities.

Our second case study attempts a pure algorithm test by running the identical analysis as discussed above over a sample of final state particles sampled from individual uniform energy distributions. The high energy case (labelled Uniform HE in Tab. III) samples particle energies between 10 MeV (typical liquid argon threshold energy value) and 4500 MeV (approximately the mean Neutrino energy of the proposed CN2PY experiment), all with equal weighting factors, while the low energy option (labelled Uniform LE in Tab. III) samples up to 770 MeV (corresponding to the mean energy of the current JPARC neutrino beam). These case studies gauge the sensitivity of the method to knowledge of the beam kinematics. The proposed variables are independent of beam characteristics but the multivariate analysis step depends on these case study assumptions.

### A. Electron to combined Hadron/lepton background discrimination

Results in this section summarise the performance of the proposed discriminating variables when attempting to identify Electrons in a data sample consisting of all dominant final state particles, i.e. charged and neutral Pion, Protons, Kaons and Muons. The most straightforward way of illustrating the effectiveness of the proposed variables can be seen in Fig. 5, showing the background rejection as a function of signal efficiency for all four chosen methods, the nearest neighbour (KNN), two variations of boosted decision trees (BDT, BDTG) and a neural network (MLPBNN). These plots would ideally show a complete background rejection for all signal efficiencies up to 100%. The closer the curves follow these ideal lines on the figure, the better the discrimination of the selected MVA method. The MVA methods mentioned above have been chosen as the most effective among a list of 24 possible methods offered in the TMVA toolkit.

Quantitative results for efficiencies and purities in EM shower discrimination are given in Table III, and illustrate a successful (well above 90% efficiency and purity) analysis technique in distinguishing EM showers from Hadron showers in a LAr detector at all interesting Neutrino energies. Additionally, we note that the reduced efficiency and purity values for low energy primary neutrinos compared to the high energy neutrino case study is as expected. Finally, the method appears relatively insensitive to presence or absence of priori beam knowledge.

### B. Additional applications

The variables discussed above lend themselves to further applications simply because they are sensitive to only the geometrical shapes of clouds of hits in 3D space as opposed to kinematic variables. As a first application we consider neutral current (NC) interactions in LAr. NC interactions form an important background to Neutrino oscillation signals. The dominant detectable signature of such interactions would be the appearance of neutral Pions in an event. Due to their prompt decay into a pair of photons, with the inevitable EM showers, they constitute the most destructive background to Electron-neutrino charged-current interactions. This means that identifying final state  $\pi^0$  would be beneficial for several reconstruction tasks. One study [14] delivered a strong discrimination factor of  $10^{-3}$  for mis-identified  $\pi^0$  in a LArTPC, a number which is widely quoted. Our efforts here deliver a weaker  $\pi^0$  discrimination, see below. However it does not rely on complex computational tasks such as shower separation and fitting and subsequent vertex finding in a potentially very busy event structure, i.e. the reason why [14] relies on visual event selection.

The optimal signal and background efficiencies for the  $\pi^0$  selection are shown in Table III (see also Fig. 6 and

TABLE II: The relative weighting factors for the final state particles resulting from the CN2PY Neutrino beam containing particles given in the first column. These are each taken into account during the multivariate analysis stage. Note that Muon and Electron energy spectra are taken from Genie simulations using the corresponding neutrino-flavour weighting factor.

	$\pi^+$	$\pi^-$	$\pi^0$	p	$K^\pm$	$K^0$	$\gamma$
$\bar{\nu}_\mu$	0.203	0.508	0.409	1.610	0.016	0.022	0.035
$\nu_\mu$	$2.42 \times 10^{-2}$	$9.89 \times 10^{-3}$	$2.04 \times 10^{-2}$	$6.284 \times 10^{-1}$	$1.43 \times 10^{-3}$	$1.1 \times 10^{-3}$	$1.96 \times 10^{-3}$
$\bar{\nu}_e$	$9.4 \times 10^{-4}$	$2.32 \times 10^{-3}$	$1.85 \times 10^{-3}$	$7.2 \times 10^{-3}$	$7.7 \times 10^{-5}$	$1.1 \times 10^{-4}$	$1.8 \times 10^{-4}$
$\nu_e$	$7.6 \times 10^{-4}$	$3.1 \times 10^{-4}$	$6.4 \times 10^{-4}$	$1.95 \times 10^{-3}$	$4.5 \times 10^{-5}$	$3.4 \times 10^{-5}$	$5.7 \times 10^{-5}$

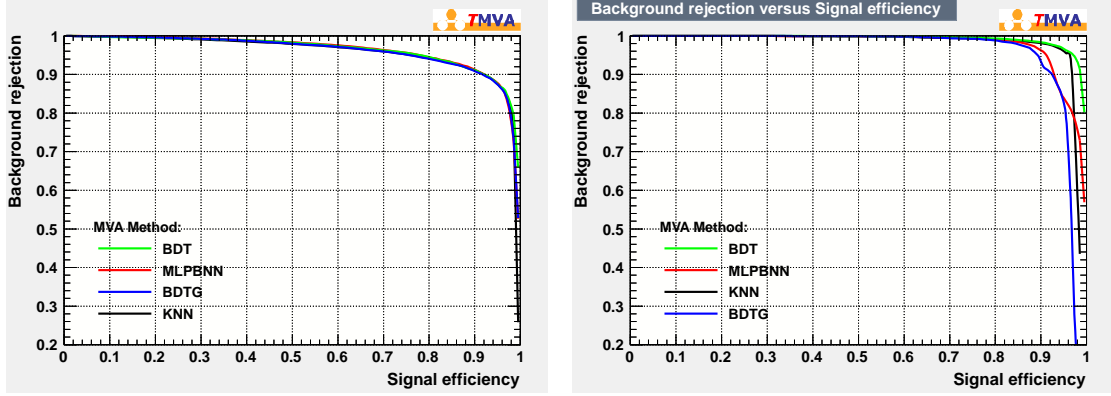


FIG. 5: Background rejection as a function of the signal efficiency for all four chosen methods for a (left panel) high energy uniform Electron energy distribution and (right panel) CN2PY beam. The methods are: the k-nearest neighbour search (KNN), two variations of boosted decision trees (BDT, BDTG) and a neural network (MLPBNN), all originating from the TMVA toolkit [4]. For numerical results on this analysis, see Table III.

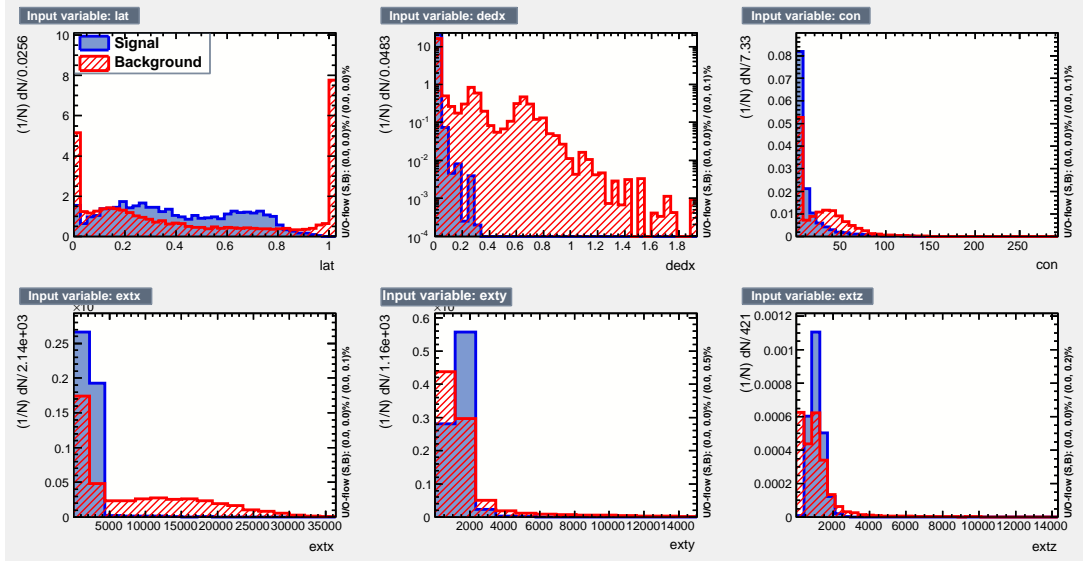


FIG. 6: Variables for a  $\pi^0$  final state particle signal from a CN2PY beam compared to the complete shower background. The final three variables describing the geometrical shape of the structures are improving the discrimination when compared to a three (the first three) variable analysis.

Fig. 7). Just as for the study on Electron to Hadron discrimination, all subsequent studies on changing the

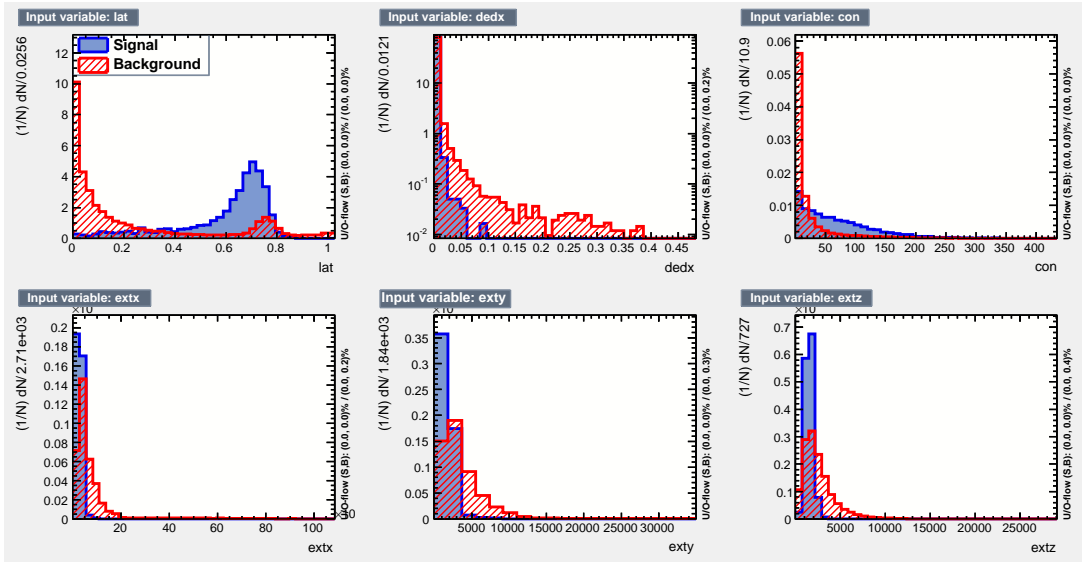


FIG. 7: Variables for a  $\pi^0$  final state particle signal from a uniform energy distribution compared to the complete shower background.

signal, here to the  $\pi^0$  particle, consider the complete set of background particles, listed as final state particles in Table II and additionally the relevant leptons, i.e. Muons and Electrons. All final state particles other than the selected signal particle constitute background.

Other final state particles can also be identified with varying degrees of success. In Table II we list results for Muon, Protons, Kaons, where charged Pion results are practically identical to Kaon results, hence have been left out.

### C. Detector threshold effects

Detector-specific effects depend heavily on our primary assumption of successful clustering of hits belonging to a single particle in an overall unspecified detector event. However, any automated analysis will at some point have to solve this challenge for finely-grained LAr detector devices.

Nevertheless, threshold variations would remove (or add) hits to the total simulated single particle event and potentially change geometrical structures. In order to test the robustness of our method against such a realistic detector effect, we studied two scenarios: one realistic hit energy cut at 120 keV/mm for quenched (measured) energies and one essentially without an hit energy cut (1 keV/mm). The threshold choice of 120 keV/mm originates from the simulated onset of the Muon energy loss peak which would be left practically fully intact by this cut. The minimal cut scenario at 1 keV/mm roughly doubles the total amount of hits for most single particles simulated.

The change from these threshold effects on all of the

particle identification results shown earlier is negligible, typically less than 0.3% on any signal or background efficiency quantity.

Similar robustness should be pointed out with respect to hit smearing effects, i.e. the case when individual hits are represented by more realistic volumes of three to six mm cubes (or even asymmetric dimensions). Our proposed variables are purely measures of the geometry of structures in a LArTPC. As long as the smallest spatial measure, i.e. a hit, is small compared with the extent of shower/track structures, we do not expect any of our analysis results to change significantly.

## IV. CONCLUSION

We have presented a study identifying particles in event structures obtained in high-granularity detectors such as a liquid argon TPC using six discriminating variables. Combining them using MVA algorithms from the TMVA toolkit gives signal efficiencies for Electron and Muon identification well above 90% with high purities on all Neutrino interaction channels. Protons, Kaons and charged Pions (not discussed above due to very similar results to Kaons) show anything from acceptable to poor purity but high efficiency. Neutral Pion identification can be made very efficient if a purity between 16% and 25%, depending on the initial Neutrino energy, is not a concern.

The data used in this work has been assumed to consist of hits containing three spatial coordinate values and one energy value, which should be the case for LAr TPC detectors. Furthermore, it is assumed that each single structure to be analysed has been clustered correctly



TABLE III: Particle identification efficiencies and contamination (background efficiency or 'contamination' is equal to 1.0 - signal purity) in a combined background of Hadron showers and Muons for all selected MVA methods. Efficiencies are calculated for the optimal decision boundary values defined by maximising the signal-to-total event ratio,  $S/(S+B)$ .

MVA method	Beam case study	Particle Signal/Background efficiency [%]				
		Electron	$\pi^0$	Muon	Proton	Kaon
KNN	CN2PY	95.3 / 4.2	96.3 / 18.2	97.7 / 1.2	88.7 / 26.7	93.9 / 26.0
MLPBNN	CN2PY	90.6 / 4.1	95.4 / 21.3	96.4 / 2.6	69.6 / 6.8	92.3 / 22.8
BDT	CN2PY	96.7 / 4.5	96.9 / 16.6	98.3 / 1.4	95.7 / 34.0	93.6 / 22.6
BDTG	CN2PY	89.1 / 4.5	96.3 / 24.5	95.0 / 1.2	87.6 / 25.8	92.3 / 21.7
KNN	Uniform HE	96.2 / 13.9	95.0 / 18.9	97.7 / 2.8	96.6 / 60.0	95.7 / 49.2
MLPBNN	Uniform HE	95.4 / 12.5	93.2 / 24.1	96.3 / 4.7	95.9 / 62.8	95.6 / 50.8
BDT	Uniform HE	96.6 / 14.0	95.9 / 21.5	98.5 / 3.0	97.5 / 64.3	95.7 / 48.8
BDTG	Uniform HE	95.7 / 13.4	94.4 / 27.0	97.5 / 2.4	97.7 / 61.7	95.7 / 48.0
KNN	Uniform LE	90.0 / 17.1	92.0 / 28.3	91.0 / 17.5	94.5 / 65.4	90.3 / 27.9
MLPBNN	Uniform LE	90.5 / 19.1	93.1 / 32.8	86.1 / 14.4	91.9 / 60.0	91.4 / 29.7
BDT	Uniform LE	91.3 / 19.5	94.6 / 30.8	91.2 / 16.7	91.6 / 43.0	91.4 / 29.3
BDTG	Uniform LE	91.0 / 17.5	93.4 / 30.5	91.7 / 16.9	89.3 / 41.0	90.0 / 27.5

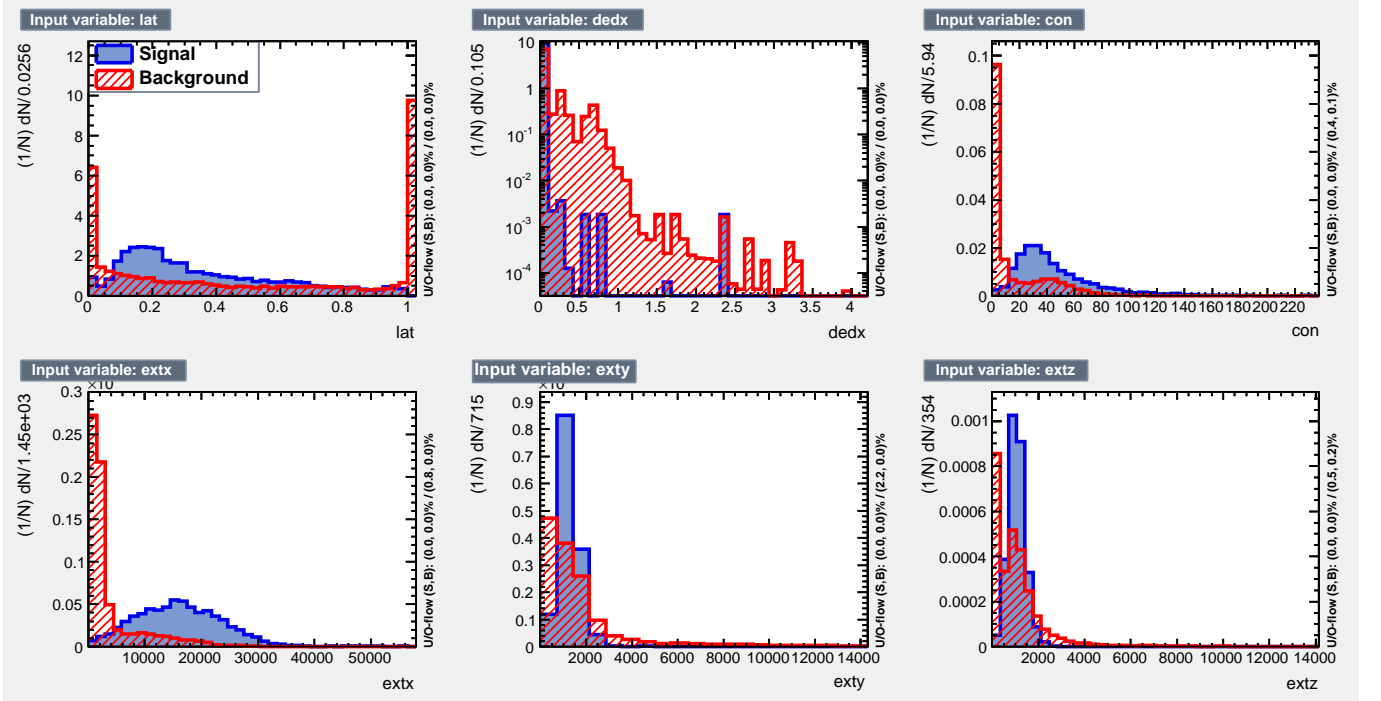


FIG. 8: Similar to Fig. 1 for the CN2PY beam producing Muons in the final state, here defined as signal compared to the complete shower background.

which is still an outstanding challenge for automated data analysis on high granularity detector data. Nevertheless, if such a clustering can be achieved by some means, then this work proposes an efficient and reliable method to identify Electron (as well as positron) events in a combined hadronic and leptonic background. These would be the primary signatures of charged cur-

rent Electron-Neutrino interactions which constitute the main target of future long baseline experiments. It also allows the identification of neutral Pions without additional knowledge of decay vertices (or similar quantities) in a mixed background of other Hadrons and leptons, and can be used for Muon identification and as an efficient first pass on Proton, Kaon and charged Pion identifica-



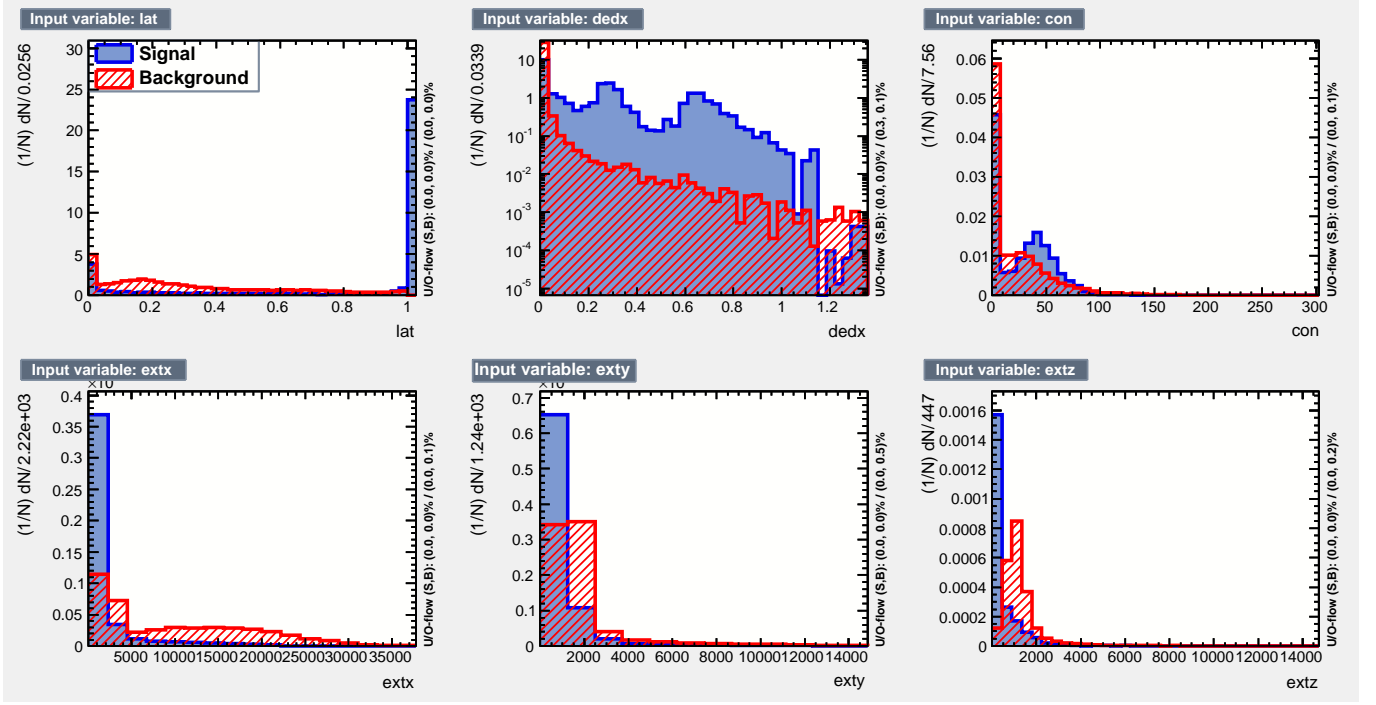


FIG. 9: Similar to Fig. 1 for the CN2PY beam producing Protons in the final state, here defined as signal compared to the complete shower background.

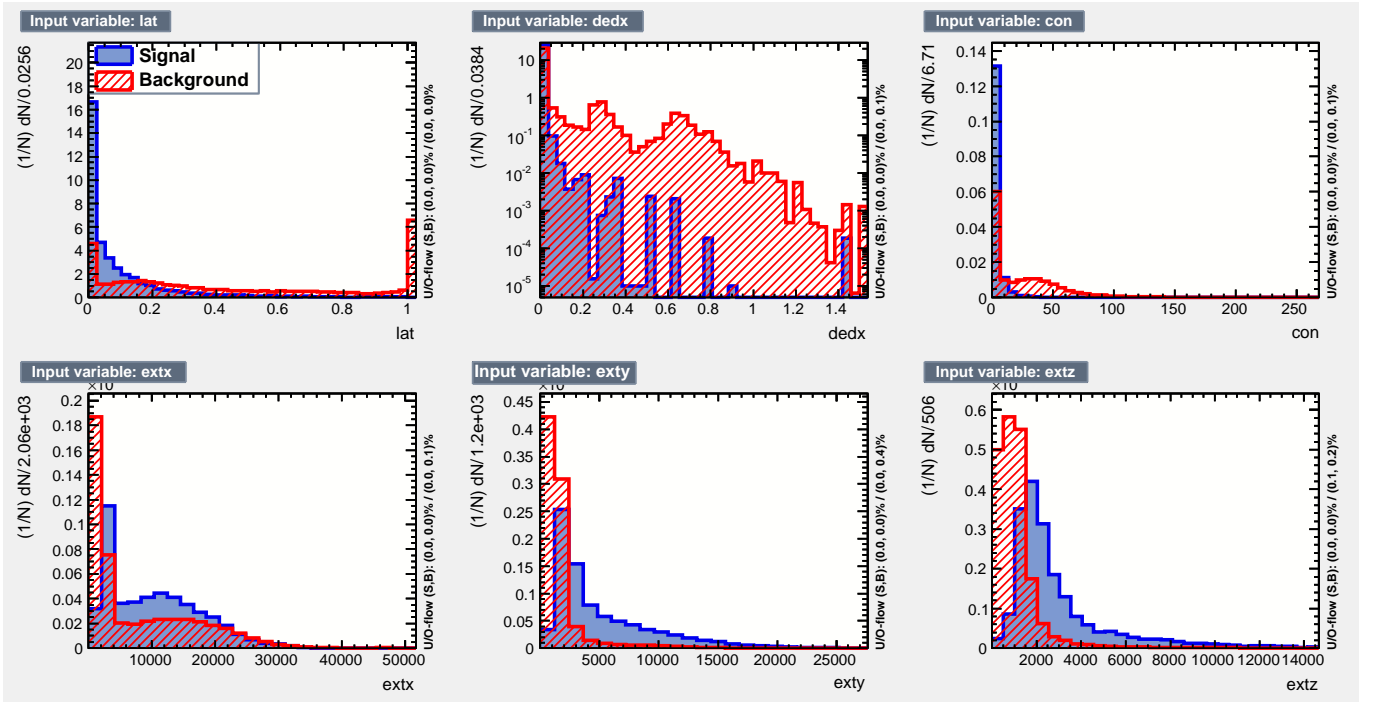


FIG. 10: Similar to Fig. 1 for the CN2PY beam producing Kaons (charged and neutral combined) in the final state, here defined as signal compared to the complete shower background.

tion.

## Acknowledgments

We acknowledge the contribution made to this study by Timothy Hughes and Laurence Woodward who

worked with the corresponding author as final year project students on this topic. Support on the EU-FP7

funded programme LAGUNA/LBNO is also acknowledged.

- 
- [1] A. Rubbia, J. Phys., Conf. Ser. **308**, 012030 (2011); B. Fleming, J. Phys., Conf. Ser. **308**, 012007 (2011); M. Tanaka, J. Phys., Conf. Ser. **308**, 012022 (2011).
  - [2] C. Rubbia *et al.*, JINST **6** P07011 (2011).
  - [3] I. T. Jolliffe, *Principal Component Analysis*, Springer, 2<sup>nd</sup> ed., New York (2002).
  - [4] P. Speckmayer, A. Hoecker, J. Stelzer and H. Voss, J. Phys., Conf. Ser. **219**, 032057 (2010).
  - [5] B. Andrieu *et al.*, Nucl. Instrum. Methods Phys. Res., Sect. A **344**, 492 (1994).
  - [6] E. Aprile, A. E. Bolotnikov, A. I. Bolozdynya and T. Doke, *Noble Gas Detectors*, Wiley-VCH, Weinheim (2006).
  - [7] C.B. Barber, D.P. Dobkin and H.T. Huhdanpaa, ACM Trans. on Mathematical Software, **22**, 469 (1996).
  - [8] T. E. Oliphant, Comput. Sci. Eng. **9**, 10 (2007).
  - [9] A. Ereditato and A. Rubbia, Nucl. Phys. B (Proc. Suppl.) **154**, 163 (2006); E. F. Martinez, T. Li, S. Pascoli and O. Mena, Phys. Rev. D **81**, 073010 (2010).
  - [10] A. Longhin, PoS (ICHEP 2010) 325.
  - [11] C. Andreopoulos, Nucl. Instrum. Methods Phys. Res., Sect. A **614**, 87 (2010).
  - [12] S. Agostinelli *et al.*, Nucl. Instrum. Methods Phys. Res., Sect. A **506**, 250 (2003).
  - [13] S. Amoroso *et al.*, Nucl. Instrum. Methods Phys. Res., Sect. A **523**, 275 (2004).
  - [14] A. Ankowski *et al.*, ICARUS coll., Acta Phys. Polon. **B41**, 103 (2010).